International Journal of Biological Macromolecules 280 (2024) 135510

Contents lists available at ScienceDirect

International Journal of Biological Macromolecules

journal homepage: www.elsevier.com/locate/ijbiomac

Structural dynamics of the TPR domain of the peroxisomal cargo receptor Pex5 in *Trypanosoma*

Michal Banasik [a,1], Valeria Napolitano [a,b,1], Artur Blat [a,c], Karim Abdulkarim [a,d], Jacek Plewka [a,j], Cezary Czaplewski [e,f], Artur Gieldon [e], Maciej Kozak [g,h], Benedykt Wladyka [k], Grzegorz Popowicz [i], Grzegorz Dubin [a,*]

[a] *Malopolska Centre of Biotechnology, Jagiellonian University, Gronostajowa 7a, 30-387 Krakow, Poland*
[b] *Department of Microbiology, Faculty of Biochemistry, Biophysics and Biotechnology, Jagiellonian University, Gronostajowa 7, 30-387 Krakow, Poland*
[c] *Doctoral School of Exact and Natural Sciences, Jagiellonian University, Krakow, Poland*
[d] *Department of Biology, College of Science, Salahaddin University-Erbil, Kirkuk Road, 44002 Erbil, Kurdistan Region, Iraq*
[e] *Faculty of Chemistry, University of Gdansk, Wita Stwosza 63, 80-308 Gdansk, Poland*
[f] *School of Computational Sciences, Korea Institute for Advanced Study, 85 Hoegiro Dongdaemun-gu, Seoul 02455, Republic of Korea*
[g] *Faculty of Physics, Adam Mickiewicz University, 61-614 Poznan, Poland*
[h] *National Synchrotron Radiation Centre SOLARIS, Jagiellonian University, 30-392 Kraków, Poland*
[i] *Helmholtz Zentrum München, Neuherberg, Germany*
[j] *Department of Organic Chemistry, Faculty of Chemistry, Jagiellonian University, Gronostajowa 2, 30-387 Krakow, Poland*
[k] *Department of Analytical Biochemistry, Faculty of Biochemistry, Biophysics and Biotechnology, Jagiellonian University, Gronostajowa 7, 30-387 Krakow, Poland*

ARTICLE INFO

Keywords:
PEX5
Peroxin
TPR domain
Trypanosoma
Chagas disease
Structural dynamics

ABSTRACT

Peroxisomal protein import has been identified as a valid target in trypanosomiases, an important health threat in Central and South America. The importomer is built of multiple peroxins (Pex) and structural characterization of these proteins facilitates rational inhibitor development. We report crystal structures of the *Trypanosoma brucei* and *T. cruzi* tetratricopeptide repeat domain (TPR) of the cytoplasmic peroxisomal targeting signal 1 (PTS1) receptor Pex5. The structure of the TPR domain of *Tb*Pex5 represents an apo-form of the receptor which, together with the previously determined structure of the complex of *Tb*Pex5 TPR and PTS1 demonstrate significant receptor dynamics associated with signal peptide recognition. The structure of the complex of TPR domain of *Tc*Pex5 with PTS1 provided in this study details the molecular interactions that guide signal peptide recognition at the atomic level in the pathogenic species currently perceived as the most relevant among Trypanosoma. Small – angle X – ray scattering (SAXS) data obtained in solution supports the crystallographic findings on the compaction of the TPR domains of *Tb*Pex5 and *Tc*Pex5 upon interaction with the cargo.

1. Introduction

Trypanosoma brucei and *Trypanosoma cruzi* are human pathogens responsible for sleeping sickness in sub-Saharan Africa and Chagas disease in Central and South America, respectively. While the former disease has been largely eradicated through preventive measures, Chagas disease remains a significant health threat with an estimated 10 million affected individuals worldwide [1]. Only a limited number of treatment options against Chagas disease are currently available. Moreover, the treatment approaches are relatively effective in the early, acute phase, but the efficacy dramatically drops in the chronic stage of the disease. Thus, novel drug targets and drug candidates are of immediate need [2].

Trypanosomatids exhibit a complex life cycle where the parasite is transferred between human hosts by blood-feeding insects, while within the host it cycles between the bloodstream and organs including the gut, brain, skin and adipose tissue [3,4]. Unlike other eucaryotes, the glucose metabolism of *Trypanosoma* is uniquely compartmentalized in membrane-bound organelles known as glycosomes (specialized peroxisomes). The organelles lack protein production abilities and import proteins from the cytoplasm. Peroxisomal protein import is a valid drug target in trypanosomiasis [5]. The transport is mediated by a multiprotein peroxin system [6]. The protein cargo is first recognized by the

* Corresponding author at: Malopolska Centre of Biotechnology of the Jagiellonian University, Gronostajowa 7A, 30-387 Krakow, Poland.
E-mail address: grzegorz.dubin@uj.edu.pl (G. Dubin).
[1] Equal contribution.

https://doi.org/10.1016/j.ijbiomac.2024.135510
Received 24 June 2024; Received in revised form 6 September 2024; Accepted 7 September 2024
Available online 18 September 2024

cytoplasmic receptor Pex5, specifically, by its C – terminal tetratricopeptide repeat (TPR) domain. The complex is tethered to the membrane by the interaction with the transmembrane receptor Pex14 and translocated into the glycosome lumen with the help of Pex13. Additional peroxins regenerate the system. The mechanisms of translocation and system regeneration remain in vivid research [7]. Most interestingly, unlike other transporters, the Pex system mediates the transfer of folded proteins [6,8].

Cargo recognition by human Pex5 is relatively well understood [9]. By virtue of its TPR domain, the Pex5 receptor recognizes a peroxisomal targeting signal 1 label (PTS1) on the cargo. The PTS1 label consists of a C-terminal tripeptide with a consensus Ser-Lys-Leu sequence. The TPR domain of human Pex5 (*Hs*Pex5) consists of seven TPRs (helix-turn-helix) motifs [10,11] and such motifs are commonly involved as mediators of protein – protein interactions [12]. Initial descriptions reported rigidly arranged TPR1–3 (three consecutive TPR domains) and TPR5–7 domains connected by a partially distorted TPR4 domain. The very C-terminal end of the Pex5 protein forms a three-helix bundle where the arrangement of two helices resembles that found in a classical TPR motif. The C-terminal region is connected to the TPR7 motif through a flexible 7-C-loop, which is poorly defined by the electron density in the available structures. Four conserved residues (N415/526/534/561) contributed by TPRs 4, 5, 6, and 7 play a crucial role in the interaction between Pex5 and PTS1 in human Pex5. It has been proposed that the C-terminal helical bundle forms a second, cargo specific, binding site [13], but the hypothesis requires further experimental evidence.

Crystal structures of apo- and PTS1 ligand-containing TPR domain of *Hs*Pex5 [10,13,14] indicated significant structural rearrangements related to binding. An open, "snail-like" arrangement of the apo-form transforms into a closed, "ring-like" conformation upon ligand interaction. In the first approximation, TPR4 provides a hinge for the coordinated closing movement of the rigid TPR1–3 and TPR5–7 domains [10]. However, a closer examination shows additional bending in other regions of the protein, shifting of TPR5 and 6 with respect to TPR1–3 and changes in the conformation of the 7-C-loop [11]. Furthermore, the comparison of available crystal structures of the apo *Hs*Pex5 TPR domain indicates significant flexibility within the apo structure itself.

Targeting Pex5 is a promising strategy in human African trypanosomiasis and Chagas disease, however, the lack of structural information complicates inhibitor design. Here, we deliver high resolution structural information and analyze the structural dynamics of PTS1 recognition by the TPR domain of Pex5 ($Pex5_{TPR}$) in *Trypanosoma* facilitating future efforts of antiparasitic drug development.

2. Materials and methods

2.1. Protein expression and purification

The coding sequence of the C – terminal TPR domain of *T. brucei* Pex5 (amino acids: 332–655; Gene ID: 3657219) fused with a TEV protease recognition site was chemically synthesized and cloned into the pET24a+ plasmid between *Eco*RI and *Xho*I sites in – frame with a histidine tag (GenScript). The codon – optimized coding sequence of the TPR domain of *T. cruzi* Pex5 (amino acids: 347–668; Gene ID: 3548236) was obtained from Integrated DNA Technologies and cloned between *Nco*I and *Not*I sites of the pETHSU vector in – frame with N-terminal histidine and SUMO tags (see Supporting Information for the exact sequences of the constructs).

For protein expression the constructs were transformed into *E. coli* BL21(DE3). Bacteria were cultured at 37 °C in LB medium and induced in the mid – log phase with 1.0 mM IPTG. Following induction, the culture was continued overnight at 18 °C. Bacteria were collected by centrifugation, the pellets were suspended in the lysis buffer (50 mM Hepes pH 7.5, 300 mM NaCl, 20 mM Imidazole, 10 mM β-mercaptoethanol, 40 μM AEBSF and 1 μg/ml DNAase I) and lysed by sonication. Lysates were cleared by centrifugation and the protein of interest was recovered on Ni – NTA agarose (Qiagen). After extensive washing with the lysis buffer, *Tb*$Pex5_{TPR}$ was eluted with the lysis buffer containing 300 mM imidazole. The histidine tag was removed using His-TEV protease while dialyzing into the lysis buffer. The protease and the tag were removed by negative chromatography on Ni – NTA agarose. *Tc*$Pex5_{TPR}$ was released from the affinity column by overnight digestion with dtUD1 protease. The proteins of interest were further purified, and the buffer exchanged by gel filtration on Superdex 75 (16/60) (GE Healthcare) in the crystallization buffer (20 mM Hepes, pH 7.5; 100 mM NaCl and 5 mM β-mercaptoethanol).

2.2. Crystallization and data collection

Tb$Pex5_{TPR}$ was concentrated to 8.0 mg/ml by ultrafiltration. Screening for crystallization conditions was performed using the sitting-drop vapor diffusion approach and commercially available buffer sets. Crystals were obtained in 0.9 M sodium-potassium tartrate tetrahydrate, 20 % w/v glycerol, 0.05 M HEPES pH 7.4 after 8 days at 20 °C and after 20 days at 4 °C.

Tc$Pex5_{TPR}$ – PTS1 protein-ligand complex was prepared by mixing 1 mg/ml of protein with a 5-fold molar excess of PTS1 (YQSKL). The complex was concentrated to 8.0 mg/ml and washed several times with fresh crystallization buffer to remove the excess of PTS1. Screening for crystallization conditions was performed as described for *Tb*$Pex5_{TPR}$. Diffraction quality crystals were obtained in 0.2 M $MgCl_2$, 0.1 M Tris pH 8.5 and 30 % (w/v) PEG 4000 after random micro-seeding using Oryx8 [15] and crystals from the initial screen as seeds.

Crystals were cryoprotected in 25 % glycerol (for *Tb*$Pex5_{TPR}$) and in 25 % (v/v) ethylene glycol (for *Tc*$Pex5_{TPR}$) in the reservoir buffer and flash – cooled in liquid nitrogen. The data were collected at BESSY II 14.1 beamline operated by Helmholtz-Zentrum Berlin für Materialen und Energie (HZB, Germany) and IO2 beamline at the Diamond Light Source (Oxfordshire, United Kingdom) for apo-*Tb*$Pex5_{TPR}$ and *Tc*$Pex5_{TPR}$-PTS1, respectively.

2.3. X-ray structure determination

The data were integrated using XDS [16], and merged and scaled with Aimless [17]. The structures were solved by molecular replacement with Phaser [18] using PDB ID: 3CV0 and 3CVQ as search models for *Tb*Pex5 and *Tc*Pex5 TPR domains, respectively [11]. The molecular replacement search in *Tb*$Pex5_{TPR}$ data was only possible after splitting the TPR domain derived from the structure of a complex of *Tb*Pex5 TPR – PTS1 into two rigid body domains covering helices 1A-3B (Pro352-Leu445) and 4B—7B (Pro479-Gln598) and performing individual searches with each domain. Structures were refined through iterative cycles of interactive refinement using WinCoot [19] and automated refinement using REFMAC5 [20]. The water molecules were added using WinCoot and inspected manually. Throughout the refinement, 5 % of the reflections were used for cross-validation analysis [21] and the behavior of R_{free} was employed to monitor the refinement strategy. Data collection and refinement statistics are summarized in Table S1. The coordinates and structure factors for the *Tc*$PEX5_{TPR}$ complexed with PTS1 and *Tb*$PEX5_{TPR}$ were deposited in the Protein Data Bank with access codes 8OS1 and 9F8W, respectively.

2.4. DynDom analysis

DynDom [22] allows the structural comparison of protein conformers by analyzing two structures of a biomolecule for domain movements. Rigid domains are identified, and the relative motions of the domains are defined as hinge axes. The algorithm is implemented on an online server (http://dyndom.cmp.uea.ac.uk/dyndom/). For analyzing conformational transitions, in this study, the minimum domain size was set to 20 residues and the segment length for initial clustering (window length parameter) was set to 5 residues.

2.5. Molecular dynamics

The UNRES force field was used in molecular dynamics simulation. In this simplified model of a polypeptide chain, each amino-acid residue is reduced to two interaction sites – a united peptide group and a united side chain [23,24]. Molecular dynamics simulations with coarse-grained models offer a tremendous advantage over all-atom approaches in terms of computation speed and the exploration of conformational changes in proteins. Depending on the system size, UNRES simulations are 6 to 12 times faster than all-atom simulations in an explicit solvent using the same time step with the highly optimized GROMACS code. Additionally, the time step in UNRES can be about 2.5 times longer than in all-atom MD without violating the stability of the integration algorithm. Moreover, due to the elimination of fine-grain degrees of freedom, events occur about 1000 times faster than in all-atom simulations. The time scale of UNRES molecular dynamics is extended by 1000 to 10,000 times compared to the all-atom model. This longer time scale allows for a much wider exploration of conformational changes in proteins [25,26].

To study the structural details of the transition of the protein between two stable stages, attractive terms of the Lorentzian were utilized. Two Lorentzian attractive interactions provide a double-well potential with a bounded energy barrier [27]. The intrinsic nature of the boundedness of the Lorentzian function enables many conformational interconversions without introducing any additional biasing forces. Restraints were imposed on all parts of the system except for those that change during the conformational transition. To ensure that the transition occurs, the double-well function was used to alter the relative depth of the two wells. See Eq. (1)

$$V^{umb}(x;a,x_1x_2) = (1-a)V_1(x-x_1) + aV_2(x-x_2) \quad (1)$$

where V^{umb}(x; a, x1, x2) denotes the complete double-well function, V_n(x) denotes the Lorentz – like restraint functions centered at the n-th ($n = 1$ or 2) conformational state, x_n denotes the coordinates of the respective boundary structures, and $0 \leq a \leq 1$ is a parameter that switches the total restraint potential between the two states. In this study, we decided arbitrarily that both conformations can occur with the same probability (the "a" coefficient was set to 0.5). This method was previously successfully applied to biological systems [28].

The conformational states were defined by open and closed crystal structures (from this study and PDB ID: 3CVQ). The missing loop fragment was modeled using AlphaFold2 by DeepMind [29]. The complete protein sequence was used as input for AlphaFold2 to build the protein model. The missing loop fragment, along with its anchor residues, was extracted from this model. Using the anchor residues for alignment, the loop fragment was inserted into the crystal structure to fill the missing residues. The hybrid structure was converted to a united residue model using Ca atoms and the centers of each side chain. After the united-residue MD simulations, the back-conversion from the united residue representation to the all-atom model was performed using Pulchra software [25].

Principal Component Analysis (PCA) was used, as implemented in ProDy package [30] to extract the most significant motions. PCA is an implementation of Normal Mode Analysis (NMA) and is an efficient method to identify all collective motions of a molecular system. NMA is based on the mathematical concept that displacements of atom coordinates of the molecular system from those of the average structure are expressed as a linear combination of normal mode coordinates. The normal modes are obtained as eigenvectors of the variance - covariance matrix of coordinates obtained from the molecular dynamics trajectory [31,32].

2.6. Small angle X-ray scattering (SAXS)

SAXS data for the *Tb*Pex5 and *Tc*Pex5 TPR domains in the apo form and in complex with PTS1 were collected at the BM29 beamline at ESRF, France [39]. *Tb*Pex5$_{TPR}$ apo was measured at 5 mg/ml in batch mode, while other samples were measured in SEC – SAXS mode using an AdvanceBio SEC 300 column (0.1 ml injection, 7.5 mg/ml, 0.16 ml/min flow-rate) in 20 mM Hepes pH 7.5, 100 mM NaCl, 5 mM β-ME. The data were analyzed using CHROMIXS [33] and the Primus software from the ATSAS package. The scattering profiles were automatically assigned using the elution peaks, background subtracted on the buffer and averaged. The ATSAS software package was used to analyze the resulting scattering data to derive typical SAXS – related parameters, such as radius of gyration, maximal diameter, *etc*. The molecular envelopes were determined using 10 rounds of DAMMIF, followed by envelope averaging using DAMAVER and a final DAMMIN run.

2.7. Accession numbers

The coordinates and structure factors of apo *Tb*PEX5$_{TPR}$ and *Tc*PEX5$_{TPR}$ in complex with PTS1 were deposited in the Protein Data Bank with access codes 9F8W and 8OS1, respectively.

3. Results

To provide structural information and to assess the presumed dynamics associated with PTS1 signal recognition by Pex5 receptor in *Trypanosoma* we have expressed, purified, crystallized, and solved the structures of the C-terminal tetratricopeptide repeat domains of *Trypanosoma brucei* and *Trypanosoma cruzi* Pex5 (*Tb*Pex5$_{TPR}$ and *Tc*Pex5$_{TPR}$, respectively).

3.1. The overall crystal structure of the TPR domain of TbPex5 in the apo form

Crystals of apo *Tb*Pex5$_{TPR}$ diffracted to a resolution of 2.35 Å. They belonged to the H3 space group and contained 2 molecules in the asymmetric unit. The major part of the polypeptide chain of each molecule was well described by the electron density apart from the N – terminal region of molecule A and the region connecting 3B and 4B helices (amino acids 461–474 and 457–476 in chains A and B, respectively; Fig. 1A). The structure was refined to a reasonable quality (R_{free} = 0.241; Table S1).

The two molecules present in the asymmetric unit display almost identical overall folds. The TPR1–3 and TPR5–7 domains (Fig. 1A) both arrange comparably to other protein domains adopting the three TPR fold [34,35] and to the known structures of *Hs*Pex5 TPR domains. However, the two molecules contained in the asymmetric unit are not identical in the *Tb*Pex5$_{TPR}$ structure indicating conformational dynamics of the apo – protein. When TPR1 – TPR3 are aligned (rmsd = 0.5 Å for 113 matching C_α atoms) helices CT1 misalign by ~6.5 Å (Fig. S1). When TPR5–7 are aligned (rmsd = 0.4 Å for 100 matching C_α atoms), helices 1A misalign by ~2.5 Å and helices CT1 by ~3.0 Å, indicating bending motions at the connecting regions.

Another difference between the two molecules contained in the asymmetric unit relates to the orientation of N – and C – terminal regions. At the C – terminal side, the amino acids beyond CT4 helix (from Gly649) are oriented differently in models A and B (Fig. 1B). In model A, the C – terminal region folds over CT1 helix, contributing several hydrophobic interactions. In model B, the region over CT1 helix where the C – terminal is found in model A is occupied by the C – terminal of adjacent model A′ whereas the C – terminal region of molecule B extends towards a symmetry – related molecule, where it is stabilized by a single hydrogen bond and hydrophobic interactions of Met653 side chain. Because the described interactions of adjacent molecules bury an insignificant surface area, and because *Tb*Pex5$_{TPR}$ elutes as a monomer in SEC (not shown), we conclude that the intermolecular interactions observed in model B are artifacts of tight packing within the crystal and have no significant role in solution.

Compared to model A, an additional helix is present at the N-

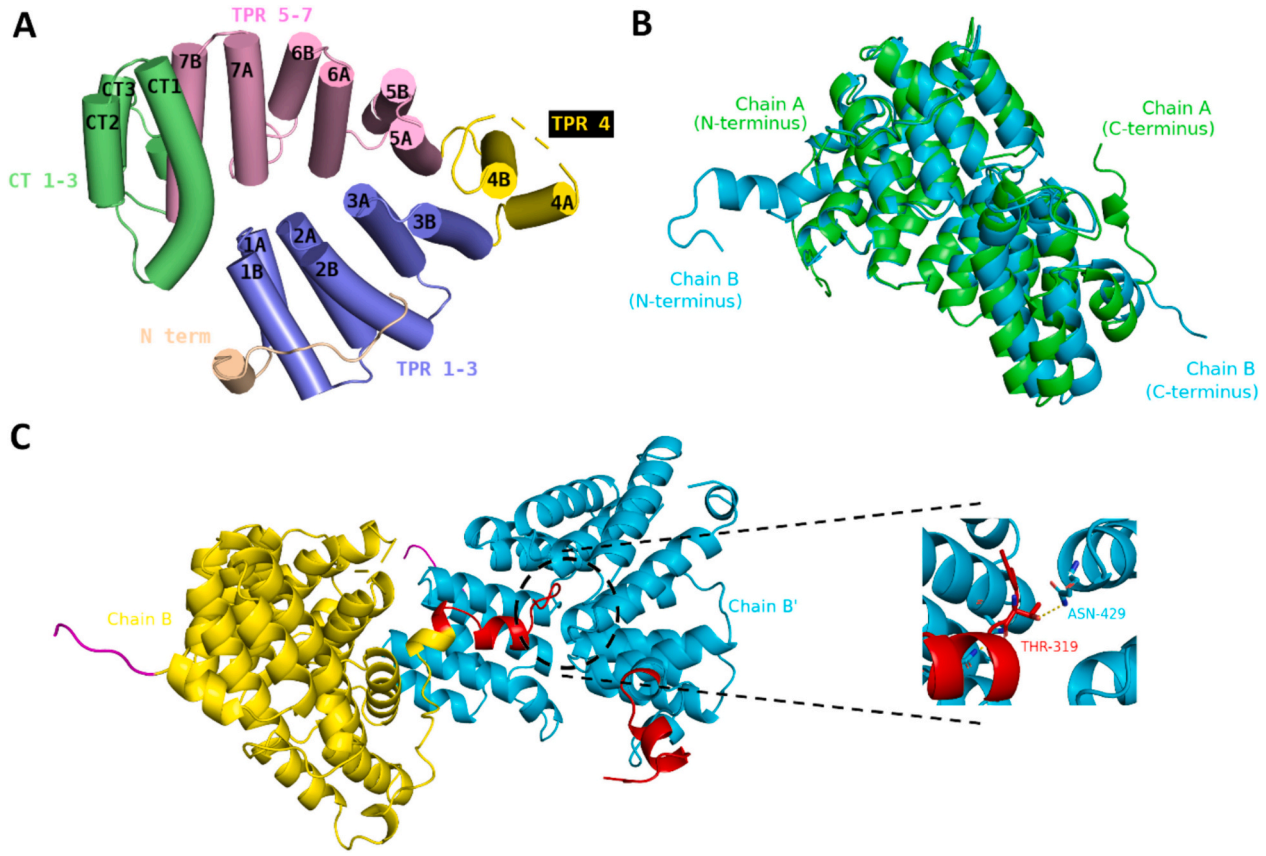

Fig. 1. Crystal structure of the TPR domain of *Tb*Pex5. (A) Schematic representation of the overall fold of the TPR domain of TbPex5. The nomenclature of secondary structure elements used in this study is indicated. (B) Structural alignment of full-length chains A and B found in the asymmetric unit within the *Tb*Pex5$_{TPR}$ crystal lattice. The overall similarity and conformational differences at the N- and C-termini are readily visible. Chain B (cyan) contains electron density defining additional helices at its N-terminus compared to chain A (green). The C-termini of both chains adopt entirely different orientations. (C) Arrangement of chain B within the crystal lattice. The N-terminal part (red) of chain B (yellow) wedges into the PTS1 binding cavity of chain B′ (cyan) from a neighboring asymmetric unit. The hydroxyl group of the Thr319 residue (magnified view, red label) contributes a hydrogen bond with the side chain of Asn429′ resembling one of the hydrogen bonds responsible for PTS1 interaction with the TPR domain of Pex5. (For interpretation of the references to color in this figure legend, the reader is referred to the web version of this article.)

terminus of model B. The helix extends away from the compact structure of the TPR domain into the direction of the symmetry – related B′ molecule, where it wedges into the PTS1 binding pocket (Fig. 1C). The interaction mimics that of PTS1 to some extent. In particular, the side chain of Met318 occupies the hydrophobic pocket accommodating the side chain of the terminal leucine in PTS1 (Fig. 2A, B). The hydroxyl of Thr319 contributes a hydrogen bond with the side chain of Asn429′ reminiscent of the interaction of the terminal carboxyl of PTS1. However, the overall disposition of the main chain and interactions other than the ones described above are not comparable. Asn429 from chain B′ (N429B′) forms a hydrogen bond through its OD1 atom with the peptide bond connecting Ser317 and Met318 of chain B, in addition to the above described interaction with Thr319B (Fig. 1C). In the PDB crystal structure 3CVL (*T. brucei* Pex5 in complex with the HEELAKL peptide, where AKL represents the PTS1 sequence), Asn429 forms a hydrogen bond with the NH group of the Lys6-Leu7 peptide bond of the PTS1-bearing peptide. The carbonyl oxygen of the peptide bond between N429B′ and E430B′ interacts with the NE2 atom of Gln323B, which in turn forms a hydrogen bond with H431B′ (Fig. 2C). The ND2 group of Asn538B′ forms a hydrogen bond with the carbonyl oxygen of the peptide bond between Thr319B and Gly320B, while in PDB: 3CVL, this ND2 group interacts with the carbonyl oxygen of the Lys6-Leu7 peptide bond in PTS1. The ND2 atom of Asn546B′ forms a hydrogen bond with the carbonyl oxygen of the Ser317B-Met318B peptide bond (Fig. 2E). The ND2 atom of Asn573B′ is hydrogen-bonded to the carbonyl oxygen of the Thr319B-Gly320B peptide bond, while its OD1 atom interacts with the NH group of the Gly321B-Gly320B peptide bond (Fig. 2E). In PDB: 3CVL, Asn573B′ ND2/OD1 forms hydrogen bonds with the carbonyl oxygen of the Lys6-Leu7 peptide bond of PTS1 and the NH group of the Glu2-Glu3 peptide bond, respectively. The OD1 atom of Asn580B′ forms a hydrogen bond with the NH group of the peptide bond connecting Glu329B and Phe330B. In PDB: 3CVL, this oxygen atom interacts with the NH group of Glu2-Glu3 peptide bond of PTS1. The OE2 atom of Glu397B′ forms hydrogen bonds with the NE2 atom of Gln322B as well as the NH group of the peptide bond between Gly321B and Gln322B. The NE2 atom of His431B′ donates a hydrogen bond to the OE1 atom of Gln323B. The OG atom of Ser615B′ forms a hydrogen bond with the NE2 atom of Gln322B (Fig. 2D). Additionally, a segment of the helix extending from model B undergoes intramolecular stiffening due to several interactions. The ND2 group of Asn334B forms a hydrogen bond with the oxygen atom of the Phe330B-Met331B peptide bond. This same oxygen atom is also hydrogen-bonded to the NH group of the peptide bond connecting Gln333B and Asn334B. A similar pattern of interactions is observed between the oxygen atom of Met331B-Leu332B peptide bond and the NH groups of the peptide bonds connecting Gln333B-Asn334B and Asn334B-Asn335B (Fig. 2F).

It should be stressed that, the N – terminal fragment in our construct, constituting the discussed helix, is composed of amino-acids not present in the *Tb*PEX5$_{TPR}$ (added in cloning). Because of this, only model A is used in further discussion, in which the central cavity is empty and the N – terminal fragment discussed above is not defined by the electron density.

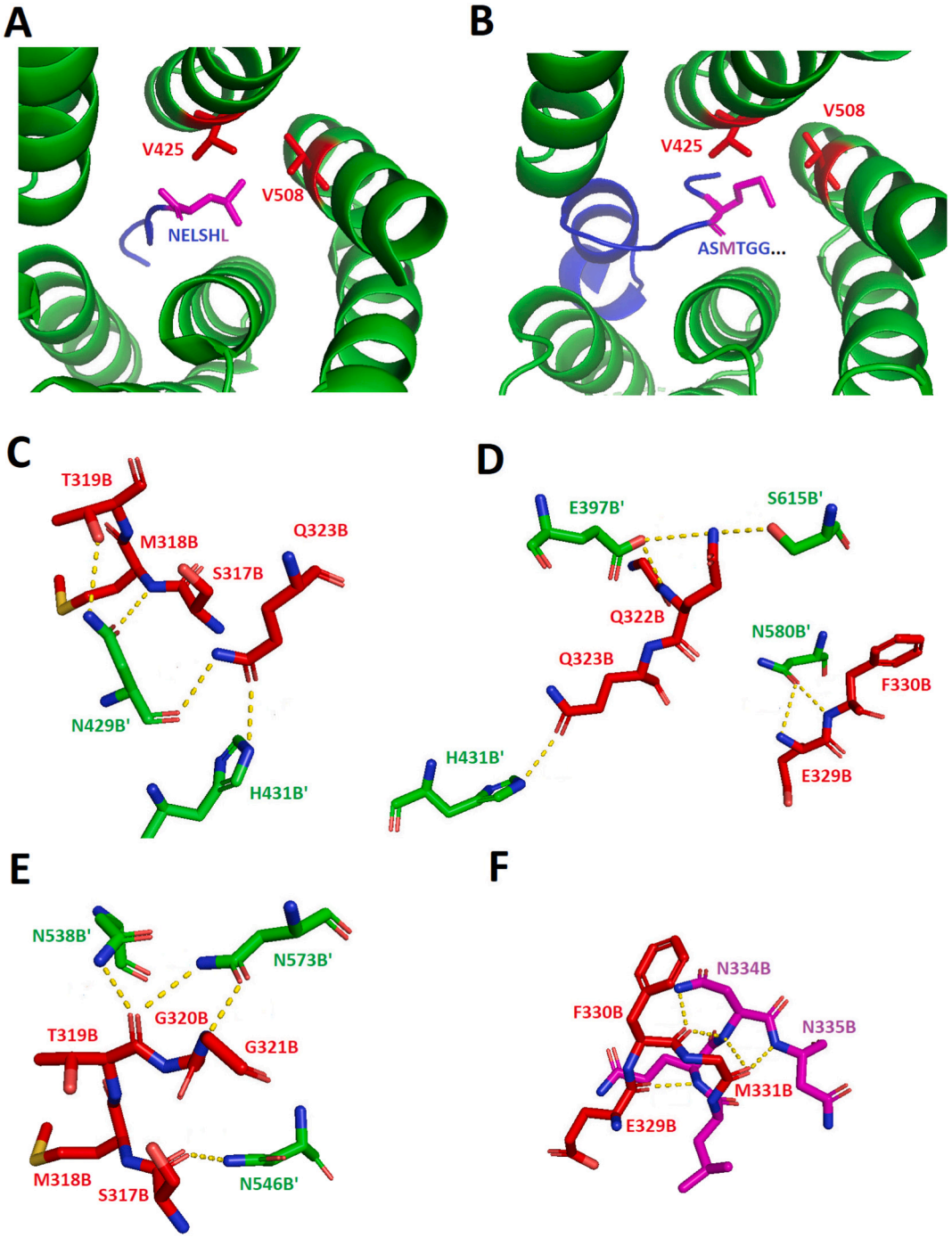

Fig. 2. Detailed interactions between model B′ and model B in the crystal structure of the *T. brucei* Pex5 protein described in this work. (A) Visualization of the location of the PTS1-terminal leucine residue, as observed in the crystal structure PDB: 3CV0 of *T. brucei* Pex5 in complex with the NELSHL peptide [11]. (B) The methionine residue from the N-terminus of chain B (M318B), as presented in this work, occupies a position within model B′ corresponding to the terminal leucine of PTS1 in (A). (C–F) Interactions between amino acid residues from model B′ of *T. brucei* Pex5 (green sticks) and residues from model B (red sticks). (For interpretation of the references to color in this figure legend, the reader is referred to the web version of this article.)

3.2. The overall crystal structure of TPR domain of TcPex5 in complex with PTS1

The best crystal of the TPR domain of TcPex5 in complex with PTS1 diffracted up to 2.10 Å resolution. The crystal belonged to the C2 space group. The asymmetric unit contained two protein molecules, both of which were well – described by well – resolved electron density, apart from helix 4A. The two molecules in the asymmetric unit are almost identical (rmsd = 0.32 Å for 296 equivalent C_α atoms). The characteristic fold of the Pex5 TPR domain is retained, with TPR1–3 and TPR5–7 constituting the lobes of a hollow oval structure, and TPR4 seemingly serving as a hinge between the two lobes. A short helical segment precedes TPR1 and provides the oval closing interactions with the C – terminal helical bundle. The overall fold of the *Tc*Pex5 TPR domain is similar to the corresponding domain of *Tb*Pex5$_{TPR}$, but significant differences in the mutual orientation of structural elements are noted, as discussed below.

3.3. Recognition of PTS1 by the TPR domain of TcPex5

The electron density corresponding to the PTS1 peptide was well – resolved, allowing for the unambiguous construction of the model in that region. The PTS1 peptide binds in a central cavity of the oval TPR domain structure, between TPR2–3 and TPR6–7 (Fig. 3A). The interaction is mediated *via* a number of hydrogen bonds, primarily contributed by asparagine residues from helices 2A, 6A and 7A, as well as hydrophobic interactions (Fig. 3B). The carboxy – terminus of PTS1 contributes four canonical hydrogen bonds with the side chains of His548, Asn551, Asn441 and Arg582. The side chain of the C – terminal leucine contributes hydrophobic interactions with the side chains of Phe536, Val521, Ala555, Lys552, Thr440 and Val437. However, the pocket accommodating the side chain of the C – terminal leucine is not a classical hydrophobic cavity, as water molecules and hydrophilic side chains are also located in the vicinity of the PTS1 – terminal leucine side chain. The orientation of the ultimate peptide bond is stabilized by a hydrogen bond contributed by the amide group with the side chain of Asn441 and hydrogen bonds between the carbonyl oxygen and side chains of Asn551 and Asn586. The side chain of the penultimate lysine contributes a single water – mediated hydrogen bond interaction with the side chain of Asp411/Glu442. Next, the penultimate peptide bond contributes a short hydrogen bond between the amine and the side chain of Asn586, while the carbonyl oxygen contributes a direct hydrogen bond with the side chain of Asn559 and a water – mediated interaction with the side chain of Asn441. Serine within the PTS1 sequence contributes two water – mediated hydrogen bonds with the side chains of Asn559 and Tyr570/Ser590/Asn586 (main chain). The main chain amine of the serine contributes a hydrogen bond with the side chain of Asn559. The side chain of glutamine proceeding the PTS1 sequence is loosely coordinated by a water – mediated hydrogen bond with the side chain of Asn441 and a direct hydrogen bond with His443/Asn441 (main chain), as well as additional direct and water – mediated hydrogen bonds within PTS1. The proceeding peptide bond provides direct and water – mediated hydrogen bond interactions with the side chains of Asn593 and Asn559, respectively. The side chain of tyrosine at position −5 (counting from the carboxy – terminal leucine) contributes hydrophobic interactions on the surface of TcPex5$_{TPR}$, including CH-π interaction with Leu632 and a sulfur/π interaction with Met635. Moreover, the hydroxyl group of tyrosine (−5) provides water – mediated interactions with Thr636 and Ser592.

3.4. Dynamic structural rearrangement of the Pex5 TPR domain upon interaction with PTS1

When comparing the crystal structure of the apo- *Tb*Pex5 TPR domain determined in this study (model A) to the structure of the corresponding TPR domain of *Tb*Pex5 in complex with the PTS peptide determined earlier (PDB ID: 3CVQ, [11]) it is immediately clear that a significant structural rearrangement is induced in the *Tb*Pex5$_{TPR}$ upon interaction with the signal peptide. A more open (snail-like) arrangement of the apo-TPR transforms into a closed (ring-like) conformation centered around the PTS1 peptide. To provide a formal description of the observed motion we used DynDom analysis [22]. Two large structural domains were identified, encompassing residues Asp337-Arg524 (domain I; TPR1-TPR5) and Asp533-Pro643 (domain II; TPR6, TPR7 and the 3-helix bundle). Each of these domains remains mostly invariant among the two compared structures. The rmsd of corresponding C_α atoms within domain I amounts to 0.9 Å for 170 matching C_α atoms and to 1.0 Å for 98 matching C_α atoms for domain II. However, the relative orientation of domains I and II is different in the compared structures. The relative displacement may be described as a 17° hinging motion with a major bending region between residues Arg525-Asp532 (connection of TPR 5 and TPR 6; Fig. 4).

Comparison of the crystal structure of the *Tc*Pex5$_{TPR}$/PTS1 complex determined in this study and that of the *Tb*Pex5$_{TPR}$/PTS1 complex determined earlier (PDB ID: 3CVQ, [11]) demonstrates high overall similarity in the structural features between both species (rmsd = 1.1 Å for 281 C_α atoms). Assuming the structure of the apo-*Tc*Pex5$_{TPR}$ resembles that of the apo-*Tb*Pex5$_{TPR}$ (and such an assumption is supported by the fact that structural differences within a bundle of available experimental apo-Pex5 TPR domain structures from different species are less than those between known apo- and PTS1 bound structures), a hinging motion comparable to that characterizing the *Tb*Pex5$_{TPR}$ would be associated with *Tc*Pex5$_{TPR}$ interaction with PTS1. However, such a conclusion remains speculative at the moment in the absence of the experimental structure of the apo-*Tc*PEX5 TPR domain.

3.5. Modeling the structural dynamics of the TPR domain of Pex5

To better understand the structural dynamics of the TPR domain of the Pex5 receptor in solution and its conformational transition upon PTS1 binding we simulated the molecular dynamics of the Pex5 TPR domain. The use of a simplified UNRES force field [23,24] allowed a long simulation span, while the utilization of the attractive terms of the

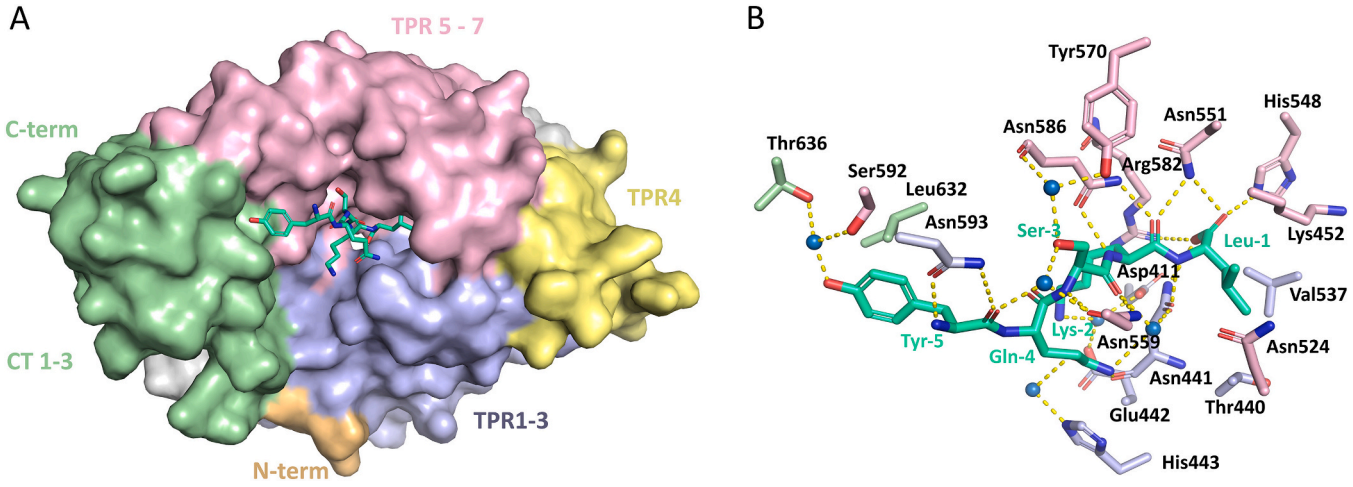

Fig. 3. Crystal structure of the TPR domain of *T. cruzi* Pex5 in complex with PTS1. (A) Overall binding mode of PTS1 (stick representation) in the cavity formed between TPR1–3 (light blue) and TPR5–7 (pink) of *Tc*Pex5$_{TPR}$ (surface representation). (B) Details of the interaction depicted in panel A. Residues involved in the binding between the TPR domain of TcPex5 and PTS1 are depicted in stick model (for color coding, refer to panel A). Water molecules mediating hydrogen bond interactions are represented as blue spheres. (For interpretation of the references to color in this figure legend, the reader is referred to the web version of this article.)

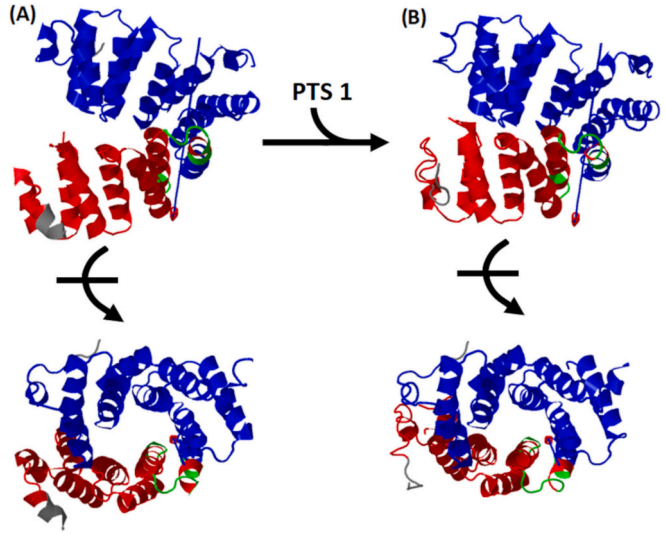

Fig. 4. Structural dynamics associated with the interaction of PTS1 with the TPR domain of *T. brucei* Pex5. Movement of the mobile rigid domain (red) with respect to the fixed rigid domain (blue) around the hinge regions (green), observed during the transition of the TPR from the open, apo-form (A; this work) to the closed, PTS1-bound form (B, PDB ID: 3CVQ, [11]) upon PTS1 ligand binding. The domains and movements as defined by DynDom [22]. (For interpretation of the references to color in this figure legend, the reader is referred to the web version of this article.)

Lorentzian kept the simulation within the boundaries of experimental data without introducing biasing forces (see 2.5).

The initial analysis of the simulation trajectories demonstrated tumbling motions (intermediate to complete transition) as well as complete transitions between the bound and unbound state (Fig. S2). Principal component analysis was used to characterize the major transitions, and the first normal mode explained ~60 % of the variance, with the following modes each explaining <6 % of the motion (Fig. S3).

The overall motion may be described as angle opening, with the vertex located slightly off the protein, resulting in the motion center on the protein being spread between loops connecting helices 6A with 6B and 6B with 7A (Fig. S3). The most distal points on the arms of the angle, the loop connecting helices 7B and CT1, and the N-terminal part of the TPR domain of Pex5 approach each other in space. In more detail, the conformational changes are a combination of two motions. The opening and closing are represented in its major part by mode 1 (Fig. 5) and additionally by a much less significant mode 4 (Fig. S4). Minor local rotation-like readjustments are represented by modes 2 and 3 affecting the fragment covering helices 7B to CT3, with the center of rotation located in the loop connecting helices 7B and CT1 (Fig. S4). After applying relevant simplification, the detailed description of the TPR domain dynamics is consistent with the results of the DynDom analysis.

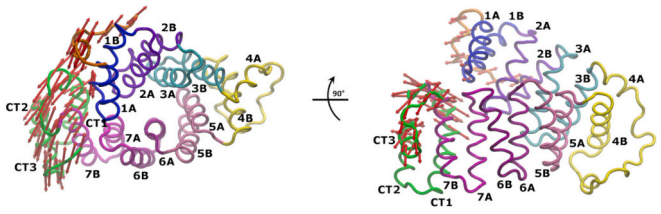

Fig. 5. Opening/closing motion of the TPR domain of Pex5 in molecular dynamics simulation. Representation of the movements associated with the first normal mode explaining almost 60 % of the entire variance observed during the simulation. Arrows indicate the moving elements without reference to the extent of the movement. For movement magnitude, refer to Fig. S3, and for following modes, refer to Fig. S4.

3.6. Assessment of the structural dynamics of the TPR domain of Pex5 in solution

The closing motion of the TPR domain around PTS1 was characterized above based on static crystal structures, which provide at best only snapshots of dynamic processes. Moreover, tight packing within the crystals may influence the protein structure to a certain extent. To assess if the observed closing motion is relevant in solution, we analyzed SAXS scattering profiles of the apo- and PTS1-bound TPR domain of Pex5 from *T. brucei* and *T. cruzi*.

Low-resolution molecular envelopes were calculated based on experimental scattering profiles (Fig. 6). Although the resolution of the obtained envelopes is too low to analyze the opening and closing of the TPR domain around PTS1, the acceptable correspondence of envelopes generated without any *a priori* structural information with crystal structures of the proteins of interest demonstrates the predictive quality of the obtained SAXS data.

Guinier analysis of the scattering profiles estimates the radius of gyration of apo-*Tb*Pex5$_{TPR}$ and apo-*Tc*Pex5$_{TPR}$ at 23.3 ± 0.1 and 23.2 ± 0.1, respectively, indicating a monomeric state in solution. The gyration radii in the presence of PTS1 (22.4 ± 0.1 and 22.5 ± 0.1 Å) are consistently ~1 Å smaller compared to the respective radii determined for the apo-TPR domains (Table S2). These results directly demonstrate that PTS1 binding induces the compaction of the Pex5 TPR domain in solution, supporting our X-ray crystallography results.

4. Discussion

The structural basis for cargo recognition by the major cytoplasmic receptor Pex5 was first revealed by the crystal structure of the TPR domain of human Pex5 in complex with the PTS1 peptide. Based on the obtained structural data, the authors suggested that ligand binding/release is associated with the hinge-like motion of TPR 1–3 and TPR 5–7 centered at TPR 4 [10]. Later crystal structures of the apo and ligand-bound forms of the TPR domain of human Pex5 allowed better sampling of the dynamics associated with ligand binding. These studies demonstrated that a “snail-like” open conformation of the apo form is converted into a “ring-like” structure of the PTS1-bound form owing to

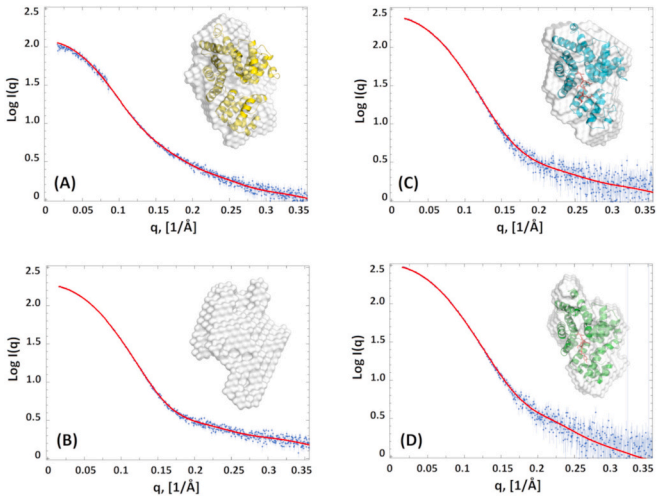

Fig. 6. The SAXS scattering profiles of apo-*Tb*Pex5$_{TPR}$ (A), apo-*Tc*Pex5$_{TPR}$ (B), PTS1-*Tb*Pex5$_{TPR}$ (C) and PTS1-*Tc*Pex5$_{TPR}$ (D). Experimental data are shown as blue dots. Molecular envelopes, calculated directly from the scattering profiles with no *a priori* assumptions, are shown in the top right corners of each panel, and the fit of the model to experimental data is depicted as a red solid line. Available high-resolution structures are fitted into molecular envelopes. (For interpretation of the references to color in this figure legend, the reader is referred to the web version of this article.)

bending/tilting motions within TPR segments 5 and 6.

Little structural information on *Trypanosoma* Pex5 was available prior to this study. No structural information on the peroxin from *T. cruzi* was available, and this study revealed for the first time the details of PTS1 recognition in the species. The structure of the TPR domain of *T. brucei* Pex5 was available in a ligand-bound form [11], but only the comparison with the structure of the apo-form obtained here revealed the dynamics related to PTS1 recognition.

The comparison of the apo-structure of *Tb*PEX5$_{TPR}$ determined in this study and the structure of the corresponding PTS1-bound structure available previously [11] allowed defining substantial dynamics of the TPR domain associated with cargo binding. The two relatively rigid structural domains, TPR 1–5 and TPR 6–7 plus the C-terminal three-helix bundle, undergo a hinging motion centered around a region connecting TPR domains 5 and 6. This observation was supported by molecular modeling.

Comparison of the apo structures of the TPR domain of *Hs*Pex5 and *Tb*Pex5 reveals significant structural correspondence. The only major difference is related to the distinct conformations of the 7-C loop, where a part of the corresponding main chain folds into a short α-helix in the *Tb*Pex5$_{TPR}$ structure, whereas it assumes an extended conformation in the *Hs*Pex5$_{TPR}$ structure. Furthermore, a global alignment of the structures is characterized by up to 2 Å shifts in positions of Cα atoms throughout the entire aligned structures. At the same time, the rigid domains, TPR1–5 and TPR 6–7 plus C-terminal three-helix bundle, overlay with much better correspondence, demonstrating that the hinging motion at the interface of TPR domains 5 and 6 is associated not only with ligand binding, but to some extent is also characteristic to the apo structure of the TPR domain itself, while PTS1 binding locks the structure in a fully closed conformation. Such a conclusion is corroborated by comparing different apo structures of the TPR domain of HsPex5, which show a range of intermediate opening angles, but none is characterized by an opening angle as low as in the PTS1 bound structure.

Crystal structures provide only snapshots of dynamic events, and the extent of the opening-closing dynamics may be broader than that seen in the static structures. Nonetheless, our SAXS data suggests that the opening motion does not result in fully extended conformations of the TPR domain of Pex5. Further analysis using site-directed labeling and FRET techniques could help better define the extent of the opening/closing movement in solution, but such experiments are beyond the scope of this study.

The mechanism locking the structure of the TPR domain of *Hs*Pex5 in a closed ring-like conformation relies on interactions of the 7-C loop with TPR 1 motif, while this interaction displaces the polypeptide chain N-terminal to TPR 1 from its position observed in the apo-structure, and the new position of this N-terminal region in the complex structure is not defined by electron density. Conversely, in *Tb*Pex5$_{TPR}$, the 7-C loop becomes partially unstructured (undefined by the electron density) in the complex structure, while the region N-terminal to TPR1 remains at the position similar to that found in both the structures of *Tb* and *Hs* apo-Pex5 TPR domains. Despite the above differences, the closing motion of TPR domains 2, 3, 5, 6 and 7 at PTS1 peptide is similar in both the *Tb* and *Hs* homologues.

The structure of the apo- TPR domain of *Tb*PEX5 provided in this study contains two protein molecules in the asymmetric unit. One of the molecules exhibits a "true" apo structure where the PTS1 cavity is empty. In the second molecule, the N-terminus of the symmetry-related model wedges into the PTS1 binding site, contributing interactions to some extent comparable to PTS1 and similarly interconnecting the two lobes of the TPR domain. This results in the conformation of the TPR domain between the apo- and PTS1 bound structure. However, the ligand in this case is unrelated to the physiological ligand (PTS1), and that is why the comparison of the two molecules contained in the asymmetric unit of *Tb*PEX5$_{TPR}$ structure is not carried beyond indicating that the structure again supports the dynamics of TPR domain and the fact that binding of any ligand is associated with the structure compaction, an observation of significance for structure-based ligand design.

Our structure of the TPR domain of *T. cruzi* Pex5 in complex with PTS1 defines for the first time the molecular architecture of the PTS1 binding pocket in the Pex5 receptor relevant for trypanosomal drug discovery. The overall binding modes of PTS1 to the TPR domain in human, *T. brucei* and *T. cruzi* receptors are almost identical, with a significant exception guiding the interaction of a crucial element of the PTS1, the C-terminal carboxylate group. In the human receptor, the carboxylate is stabilized by hydrogen bond interactions with the side chain amides of Asn415 and Asn526 and a water-mediated hydrogen bond. In the TPR domain of *T. cruzi* Pex5, histidine 548 is located at the bottom of the PTS1 binding pocket (equivalent to Leu523 in human and Gln535 in *T. brucei* TPR domains of Pex5), which histidine side chain contributes a direct hydrogen bond with the C-terminal carboxyl group of PTS1. A comparable interaction is not seen in the structure of the human complex, allowing us to expect that exploring this interaction could guide small molecule selectivity towards *T. cruzi*.

Peroxisomes have been suggested as valuable targets in trypanocidal drug discovery. Pex14 has been the first component of matrix protein delivery system which was verified as a valid target [7,36]. More recently, Pex3 – Pex19 interaction vital for protein insertion into peroxisome membrane [37] and Pex5 – cargo interactions involved in matrix protein delivery [38] have been demonstrated additional valid targets. Especially the spacious PTS1 pocket of Pex5, allowing a significant number of attachment points, seems perfect for inhibitor development. A number of small molecule inhibitors of Pex5 were identified and their docking poses were reported to resemble the binding of PTS1 [38]. These molecules can serve as scaffolds for further optimization towards potential future drugs against Chagas disease. The dynamics of the receptor unveiled in this study provides both a challenge and an opportunity in the design and optimization of specific inhibitors of Pex5-cargo interactions.

Supplementary data to this article can be found online at https://doi.org/10.1016/j.ijbiomac.2024.135510.

Funding

The experimental work was supported by grant 2017/26/M/NZ1/00797 and part of data analysis by grant 2020/39/B/NZ1/01551, both from the Polish National Science Centre (to GD). Developments within the theoretical part of molecular simulations were financed by the National Science Centre, Poland, grant 2017/26/M/ST4/00044 (to CCz). The authors acknowledge the support of the MCB Structural Biology Core Facility (funded by the TEAM TECH CORE FACILITY/2017-4/6 grant from the Foundation for Polish Science). The X-ray diffraction experiments were conducted at BESSY II 14.2 beamline at Helmholtz-Zentrum Berlin für Materialien und Energie (Berlin, Germany) and IO2 beamline at the Diamond Light Source (Oxfordshire, United Kingdom). We acknowledge the ESRF for provision of synchrotron radiation facility under proposal number MX-2341 and we would like to thank Anton Popov for assistance and support in using beamline BM29. The access to ESRF was financed by the Polish Ministry of Science and Higher Education - decision no. 2021/WK/11.

CRediT authorship contribution statement

Michal Banasik: Writing – review & editing, Writing – original draft, Validation, Software, Methodology, Investigation, Conceptualization. **Valeria Napolitano:** Writing – original draft, Validation, Software, Methodology, Investigation. **Artur Blat:** Writing – original draft, Validation, Software, Methodology, Investigation. **Karim Abdulkarim:** Methodology, Conceptualization. **Jacek Plewka:** Validation, Methodology, Investigation, Formal analysis. **Cezary Czaplewski:** Validation, Software, Methodology, Investigation, Formal analysis. **Artur Gieldon:** Validation, Software, Methodology, Investigation, Formal analysis.

Maciej Kozak: Validation, Software, Methodology, Investigation, Formal analysis. **Benedykt Wladyka:** Writing – review & editing, Validation, Methodology, Formal analysis, Conceptualization. **Grzegorz Dubin:** Writing – review & editing, Validation, Supervision, Resources, Project administration, Methodology, Funding acquisition, Data curation, Conceptualization.

Declaration of competing interest

None. The authors declare that they have no known competing financial interests or personal relationships that could have appeared to influence the work reported in this paper.

References

[1] J.R. Coura, P.A. Vinas, Chagas disease: a new worldwide challenge, Nature 465 (7301) (2010) S6–S7.
[2] C.J. Schofield, J. Jannin, R. Salvatella, The future of Chagas disease control, Trends Parasitol. 22 (12) (2006) 583–588.
[3] T.K. Smith, F. Bringaud, D.P. Nolan, L.M. Figueiredo, Metabolic reprogramming during the Trypanosoma brucei life cycle, F1000Res 6 (2017).
[4] K.M. Tyler, D.M. Engman, The life cycle of Trypanosoma cruzi revisited, Int. J. Parasitol. 31 (5–6) (2001) 472–481.
[5] V.C. Kalel, L. Emmanouilidis, M. Dawidowski, W. Schliebs, M. Sattler, G. M. Popowicz, R. Erdmann, Inhibitors of glycosomal protein import provide new leads against trypanosomiasis, Microbial Cell (Graz, Austria) 4 (7) (2017) 229–232.
[6] R. Erdmann, Assembly, maintenance and dynamics of peroxisomes, Biochimica et Biophysica Acta (BBA) - Molecular Cell Research 1863 (5) (2016) 787–789.
[7] M. Dawidowski, L. Emmanouilidis, V.C. Kalel, K. Tripsianes, K. Schorpp, K. Hadian, M. Kaiser, P. Mäser, M. Kolonko, S. Tanghe, A. Rodriguez, W. Schliebs, R. Erdmann, M. Sattler, G.M. Popowicz, Inhibitors of PEX14 disrupt protein import into glycosomes and kill *Trypanosoma* parasites, Science 355 (6332) (2017) 1416–1420.
[8] S.J. Gould, C.S. Collins, Peroxisomal-protein import: is it really that complex? Nat. Rev. Mol. Cell Biol. 3 (5) (2002) 382–389.
[9] L. Emmanouilidis, M. Gopalswamy, D.M. Passon, M. Wilmanns, M. Sattler, Structural biology of the import pathways of peroxisomal matrix proteins, Biochimica et Biophysica Acta (BBA) - Molecular Cell Research 1863 (5) (2016) 804–813.
[10] G.J. Gatto, B.V. Geisbrecht, S.J. Gould, J.M. Berg, Peroxisomal targeting signal-1 recognition by the TPR domains of human PEX5, Nat. Struct. Biol. 7 (12) (2000) 1091–1095.
[11] P. Sampathkumar, C. Roach, P.A. Michels, W.G. Hol, Structural insights into the recognition of peroxisomal targeting signal 1 by Trypanosoma brucei peroxin 5, J. Mol. Biol. 381 (4) (2008) 867–880.
[12] L.D. D'Andrea, L. Regan, TPR proteins: the versatile helix, Trends Biochem. Sci. 28 (12) (2003) 655–662.
[13] W.A. Stanley, M. Wilmanns, Dynamic architecture of the peroxisomal import receptor Pex5p, Biochimica et Biophysica Acta (BBA) - Molecular Cell Research 1763 (12) (2006) 1592–1598.
[14] W.A. Stanley, F.V. Filipp, P. Kursula, N. Schüller, R. Erdmann, W. Schliebs, M. Sattler, M. Wilmanns, Recognition of a functional peroxisome type 1 target by the dynamic import receptor pex5p, Mol. Cell 24 (5) (2006) 653–663.
[15] A. D'Arcy, F. Villard, M. Marsh, An automated microseed matrix-screening method for protein crystallization, Acta Crystallographica. Section D, Biological Crystallography 63 (2007) 550–554.
[16] W. Kabsch, XDS, Acta Crystallographica Section D 66 (2) (2010) 125–132.
[17] P.R. Evans, G.N. Murshudov, How good are my data and what is the resolution? Acta Crystallogr. Sect. D 69 (7) (2013) 1204–1214.
[18] A.J. McCoy, R.W. Grosse-Kunstleve, P.D. Adams, M.D. Winn, L.C. Storoni, R. J. Read, Phaser crystallographic software, J. Appl. Cryst. 40 (Pt 4) (2007) 658–674.
[19] P. Emsley, B. Lohkamp, W.G. Scott, K. Cowtan, Features and development of Coot, Acta Crystallographica. Section D, Biological Crystallography 66 (Pt 4) (2010) 486–501.
[20] G.N. Murshudov, P. Skubak, A.A. Lebedev, N.S. Pannu, R.A. Steiner, R.A. Nicholls, M.D. Winn, F. Long, A.A. Vagin, REFMAC5 for the refinement of macromolecular crystal structures, Acta Crystallographica Section D 67 (4) (2011) 355–367.
[21] A.T. Brünger, Free R value: a novel statistical quantity for assessing the accuracy of crystal structures, Nature 355 (6359) (1992) 472–475.
[22] S. Hayward, H.J.C. Berendsen, Systematic analysis of domain motions in proteins from conformational change: new results on citrate synthase and T4 lysozyme, Proteins: Structure, Function, and Bioinformatics 30 (2) (1998) 144–154.
[23] A. Liwo, S. Ołdziej, M.R. Pincus, R.J. Wawak, S. Rackovsky, H.A. Scheraga, A united-residue force field for off-lattice protein-structure simulations. I. Functional forms and parameters of long-range side-chain interaction potentials from protein crystal data, J. Comput. Chem. 18 (7) (1997) 849–873.
[24] A. Antoniak, I. Biskupek, K.K. Bojarski, C. Czaplewski, A. Giełdoń, M. Kogut, M. M. Kogut, P. Krupa, A.G. Lipska, A. Liwo, E.A. Lubecka, M. Marcisz, M. Maszota-Zieleniak, S.A. Samsonov, A.K. Sieradzan, M.J. Ślusarz, R. Ślusarz, P. A. Wesołowski, K. Zięba, Modeling protein structures with the coarse-grained UNRES force field in the CASP14 experiment, J. Mol. Graph. Model. 108 (2021) 108008.
[25] P. Rotkiewicz, J. Skolnick, Fast procedure for reconstruction of full-atom protein models from reduced representations, J. Comput. Chem. 29 (9) (2008) 1460–1465.
[26] A.K. Sieradzan, J. Sans-Duno, E.A. Lubecka, C. Czaplewski, A.G. Lipska, H. Leszczynski, K.M. Ocetkiewicz, J. Proficz, P. Czarnul, H. Krawczyk, A. Liwo, Optimization of parallel implementation of UNRES package for coarse-grained simulations to treat large proteins, J. Comput. Chem. 44 (4) (2023) 602–625.
[27] J. Lee, K. Joo, B.R. Brooks, J. Lee, The atomistic mechanism of conformational transition of adenylate kinase investigated by Lorentzian structure-based potential, J. Chem. Theory Comput. 11 (7) (2015) 3211–3224.
[28] A.P. Carter, C. Cho, L. Jin, R.D. Vale, Crystal structure of the dynein motor domain, Science (New York, N.Y.) 331 (6021) (2011) 1159–1165.
[29] J. Jumper, R. Evans, A. Pritzel, T. Green, M. Figurnov, O. Ronneberger, K. Tunyasuvunakool, R. Bates, A. Zidek, A. Potapenko, A. Bridgland, C. Meyer, S.A. A. Kohl, A.J. Ballard, A. Cowie, B. Romera-Paredes, S. Nikolov, R. Jain, J. Adler, T. Back, S. Petersen, D. Reiman, E. Clancy, M. Zielinski, M. Steinegger, M. Pacholska, T. Berghammer, S. Bodenstein, D. Silver, O. Vinyals, A.W. Senior, K. Kavukcuoglu, P. Kohli, D. Hassabis, Highly accurate protein structure prediction with AlphaFold, Nature 596 (7873) (2021) 583–589.
[30] Q. Cui, I. Bahar, Normal Mode Analysis: Theory and Applications to Biological and Chemical Systems, CRC Press, 2005.
[31] G.G. Maisuradze, D.M. Leitner, Free energy landscape of a biomolecule in dihedral principal component space: sampling convergence and correspondence between structures and minima, Proteins: Structure, Function, and Bioinformatics 67 (3) (2007) 569–578.
[32] L.-W. Yang, E. Eyal, I. Bahar, A. Kitao, Principal component analysis of native ensembles of biomolecular structures (PCA_NEST): insights into functional dynamics, Bioinformatics (Oxford, England) 25 (5) (2009) 606–614.
[33] A. Panjkovich, D.I. Svergun, CHROMIXS: automatic and interactive analysis of chromatography-coupled small-angle X-ray scattering data, Bioinformatics 34 (11) (2018) 1944–1946.
[34] C. Scheufler, A. Brinker, G. Bourenkov, S. Pegoraro, L. Moroder, H. Bartunik, F. U. Hartl, I. Moarefi, Structure of TPR domain-peptide complexes: critical elements in the assembly of the Hsp70-Hsp90 multichaperone machine, Cell 101 (2) (2000) 199–210.
[35] A.K. Das, P.T.W. Cohen, D. Barford, The structure of the tetratricopeptide repeats of protein phosphatase 5: implications for TPR-mediated protein–protein interactions, EMBO J. 17 (5) (1998) 1192–1199.
[36] M. Dawidowski, V.C. Kalel, V. Napolitano, R. Fino, K. Schorpp, L. Emmanouilidis, D. Lenhart, M. Ostertag, M. Kaiser, M. Kolonko, B. Tippler, W. Schliebs, G. Dubin, P. Mäser, I.V. Tetko, K. Hadian, O. Plettenburg, R. Erdmann, M. Sattler, G. M. Popowicz, Structure–activity relationship in pyrazolo[4,3-c]pyridines, first inhibitors of PEX14–PEX5 protein–protein interaction with trypanocidal activity, J. Med. Chem. 63 (2) (2020) 847–879.
[37] H. Banerjee, P. LaPointe, G. Eitzen, R.A. Rachubinski, A small molecule inhibitor of Pex3-Pex19 interaction disrupts glycosome biogenesis and causes lethality in Trypanosoma brucei, Frontiers in Cell and Developmental Biology 9 (2021) 703603.
[38] V. Napolitano, C.A. Softley, A. Blat, V.C. Kalel, K. Schorpp, T. Siebenmorgen, K. Hadian, R. Erdmann, M. Sattler, G.M. Popowicz, G. Dubin, Small molecule mediated inhibition of protein cargo recognition by peroxisomal transport receptor PEX5 is toxic to Trypanosoma, Sci. Rep. 12 (1) (2022) 14705.
[39] Mark D. Tully, Jerome Kieffer, Martha E. Brennich, Raphael Cohen Aberdam, Jean Baptiste Florial, Stephanie Hutin, Markus Oscarsson, Antonia Beteva, Anton Popov, Dihia Moussaoui, Pascal Theveneau, Gergely Papp, Jonathan Gigmes, Florent Cipriani, Andrew McCarthy, Chloe Zubieta, Christoph Mueller-Dieckmann, Gordon Leonard, Petra Pernot, BioSAXS at European Synchrotron Radiation Facility – Extremely Brilliant Source: BM29 with an upgraded source, detector, robot, sample environment, data collection and analysis software, J. Synchrotron. Radiat. 30 (2023) 258–266.